Assessment of three-dimensional biofilm models through direct comparison with confocal microscopy imaging

J.B. Xavier*, C. Picioreanu and M.C.M. van Loosdrecht

Kluyver Laboratory for Biotechnology, Delft University of Technology, Julianalaan 67, 2628 BC Delft, The Netherlands *Corresponding author (E-mail: *J.Xavier@tnw.tudelft.nl*)

Abstract The mathematical modeling of spatial biofilm formation that provides the capability to predict biofilm structure from first principles has been in development for the past six years. However, a direct and quantitative link between model predictions and the experimentally observed structure formation still remains to be established. This work assesses the capability of a state-of-the-art technique for three-dimensional (3D) modeling of biofilm structure, individual based modeling (IbM), to quantitatively describe the early development of a multispecies denitrifying biofilm. Model evaluation was carried out by comparison of predicted structure with that observed from two experimental datasets using confocal laser scanning microscopy (CLSM) monitoring of biofilm development in laboratory flowcells. Experimental conditions provided biofilm growth without substrate limitation, which was confirmed from substrate profiles computed by the model. 3D structures were compared quantitatively using a set of morphological parameters including the biovolume, filled-space profiles, substratum coverage, average thickness and normalized roughness. In spite of the different morphologies detectable in the two independent short-term experiments analyzed here, the model was capable of accurate fitting data from both experiments. Prediction of structure formation was precise, as expressed by the set of morphology parameters used.

Keywords Biofilm; confocal microscopy; 3D modeling; image analysis; model validation; morphology quantification

Water Science and Technology **Vol 49 No 11–12 pp 177–185** © IWA Publishing 2004

Introduction

Pioneer modeling approaches, developed in the 1970s, described biofilms as steady-state films with uniform biomass distribution and one-dimensional (1D) mass transport and biochemical transformations (Atkinson and Davies, 1974; Rittman and McCarthy, 1980). In the 1980s, this approach evolved to the stratified biomass multispecies/multi-substrate modeling methodology (Wanner and Gujer, 1986). This kind of model, which also only considers 1D gradients, persists to the present day as a widely used method to describe macroscopic conversions and for understanding processes in biofilm systems (Wanner and Reichert, 1996). With the recent advances in computational power and numerical methods, two-dimensional (2D) and three-dimensional (3D) approaches are now being developed (van Loosdrecht *et al.*, 2002). The new generation of models aims to explain biofilm growth by describing all factors of relevance using first principles. These new approaches contribute to understanding the role of environmental conditions in structure formation, but also the effects of lateral gradients and structural elements, such as pores, in the overall biofilm conversions. In contrast to 1D modeling, where the effect of structure is input to the model, 2D and 3D models follow a bottom-up approach where large-scale structure is resultant from actions and interactions of biomass particles at a smaller scale. The behavior of the parts at a small scale should preferentially be, in turn, defined without using assumptions of a completely hypothetical nature (van Loosdrecht *et al.*, 2002).

In these multi-dimensional approaches, mass transport and reaction of the involved chemical species are also modeled with corresponding dimensionality, i.e. 2D or 3D. Transport and reaction of chemical compounds is governed by sufficiently well known physical laws. However, the process of biomass spreading, which results from interactions

at cellular or colony scale – and is of chief importance in structure prediction – is much less understood.

In recent years, several approaches have been adopted for multi-dimensional modeling of biofilm structure. These approaches may be classified according to the methods used for (i) biomass spreading (either biomass based models, *BbM*, or individual based models, *IbM*) and (ii) diffusion and reaction of involved chemical species (either *coupled* or *uncoupled* to biomass growth). Examples of BbM approaches are the cellular automata (CA; Picioreanu *et al*., 1998) and the continuous biomass models (Dockery and Klapper, 2001; Eberl *et al*., 2001). CA, either using diffusion simulation by random walks of substrate particles (Wimpenny and Colasanti, 1997; Hermanowicz, 1999, 2001; Pizarro *et al*., 2001) or uncoupled substrate transport by diffusion solved by differential methods (Picioreanu *et al*., 1998) and by convection (Picioreanu *et al*., 1999, 2000), has so far been the most widely used approach. In CA, biomass is represented using a discrete grid, whose elements' behavior follows a simple set of rules. The IbM approach (Kreft *et al*., 1998; Kreft *et al*., 2001), computationally more demanding than CA, goes one step closer to the aim of modeling biofilm systems from first principles, by describing biomass as being composed of spherical particles with position in space defined in continuous coordinates. In IbM (Figure 1), each of the biomass particles is an individual that, throughout the process of biofilm development, grows, moves and divides (generating new individuals), but maintains its original identity. In contrast to BbM, IbM has greater potential to address questions about the relationship of microscopic and macroscopic properties in mixed-population systems (Kreft *et al*., 2001; van Loosdrecht *et al*., 2002).

Until now, most of the advanced biofilm simulations have not been directly compared to experimental predictions. In the present work, we compare experimentally observed biofilm structures to those derived from IbM simulations. Experimental observations are carried out using confocal laser scanning microscopy (CLSM), a well established technique for the non-invasive study of living, fully hydrated biofilms (Lawrence *et al*., 1998). Due to the stochastic nature of biofilm development, experimental repetitions never produce exact structural copies (Heydorn *et al*., 2000). This stochastic nature of the morphogenic process is also implemented in the biofilm models, namely using random number generation in some operations (e.g., biomass spreading). Therefore, evaluation of predicted structure cannot be carried out by direct comparison of the 3D spatial structure, and is performed here using a set of parameters for morphology quantification.

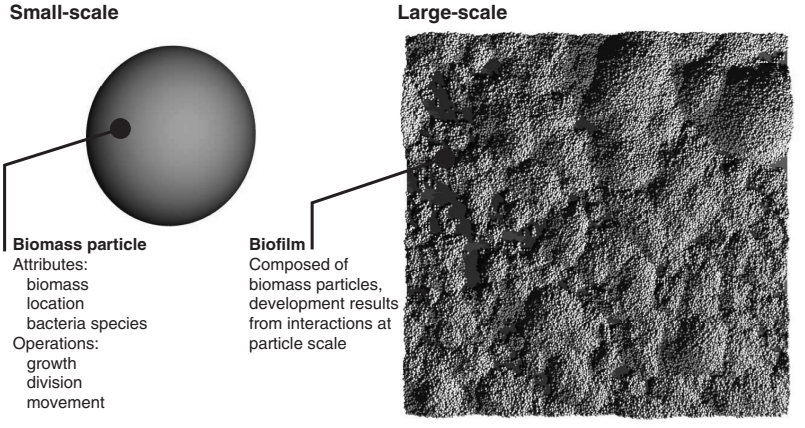

Figure 1 In individual based modeling (IbM) of biofilms, 3D structure is predicted from the small-scale interactions of spherical biomass particles

Methods

Three-dimensional modeling of biofilm structure

The 3D model for biofilm structure was implemented following the principles of individual based modeling, IbM (Kreft *et al*., 2001). The implementation of IbM used constitutes a modeling framework capable of simulating multispecies and multi-substrate systems, although for the simulations described here the multispecies system was modeled using a single-substrate system and a lumped single-species with generic properties. The IbM approach assumes biomass as being composed of individual spherical particles, each possessing its own characteristics (attributes). Biofilm growth is simulated through an iterative cycle in the course of which, at each iteration step, each biomass particle performs "actions" (operations) as a result of the environmental conditions and its internal state. The attributes and operations defining a biomass particle in this implementation of the IbM are the following:

Attributes:

- Biomass (which, in turn, defines size)
- Position in space (in continuous 3D coordinates)
- Species (defining all species specific characteristics such as growth kinetics and division parameters)

Operations:

- growth (by consuming nutrients from the surrounding medium)
- division (once a critical cell size is reached)
- movement (as a consequence of being pushed by its neighbors)

The biomass particles are formally classified as "agents with internal state", and their behavior can be thus summarized: a particle, having a given mass and located at a given position in 3D space, grows at each iterative step at a rate defined by the local substrate concentration and species-specific growth kinetics, thus increasing its own mass. Such a particle divides whenever a defined critical mass, also species-specific, is reached. Particle division results in the creation of another particle, the "daughter" of the same species, with the mass of the "mother" particle being distributed slightly unevenly between these two spheres. A particle moves whenever it is found overlapping its neighbor(s) or the solid carrier material. The shoving parameter, K_{shov}, defines the spacing among biomass particles and, therefore, biomass packing in the biofilm.

The model is stochastic, as the algorithm uses random numbers on two occasions: (i) for the random choice of direction for the placement of "daughter" particles and (ii) for the uneven division of mass between in-cell division, thus dissipating the effect of synchronous particle division in the biofilm. Spatial redistribution of biomass within the biofilm occurs by shoving of overlapped particles, as spheres divide or as they grow in size due to the biomass generation. For comparison with the experimental biofilm, a single bacterial species with generic properties was implemented using typical values for biomass density and Monod growth kinetics with single substrate limitation. The evolution of each biomass particle is governed by Eq. (1):

$$\frac{dM_{particle}}{dt} = \mu_{max}\frac{C_S}{K_S + C_S}M_{particle} \quad (1)$$

The model uncouples the substrate mass balance (diffusion-reaction processes) from the biomass spreading mechanism. Substrate concentrations in space, $C_S(x,y,z)$, are determined by solving the partial differential equations defining the substrate mass balance, including transport and reaction terms (Eq. (2)).

$$\frac{\partial C_S}{\partial t} = D_S\left(\frac{\partial^2 C_S}{\partial x^2} + \frac{\partial^2 C_S}{\partial y^2} + \frac{\partial^2 C_S}{\partial z^2}\right) + \frac{1}{Y_{XS}}\mu_{max}\frac{C_S}{K_S + C_S}C_X \quad (2)$$

The diffusion-reaction process is solved numerically to steady-state at each iteration step using the Full Approximation Storage non-linear multigrid algorithm, FAS (Press *et al.*, 1993). Although the model implementation allows the use of larger grid resolutions for computation of the substrate field, in this study a grid of 64 × 64 × 64 nodes (corresponding to grid elements of 4 × 4 × 4 μm^3) was sufficient, as determination of substrate concentrations was performed with the sole intent of confirming the initial assumption that biofilm growth was not diffusion-limited. Vertical borders of the system were implemented as cyclic boundaries. The bottom border was implemented as a zero-flux boundary for substrate diffusion and a moving upper constant value boundary was placed 10 μm above the tallest biofilm feature.

Flowcell experiments

Biofilms from a multispecies consortium were grown in laboratory flowcells and monitored using CLSM following a procedure described previously (Xavier *et al.*, 2001). The choice of a denitrifying system was aimed at simplicity, as the electron acceptor is a soluble species. The used synthetic growth medium suitable for denitrification included high concentrations of KNO_3, 5.0 $g.L^{-1}$, and KCH_3COO, 3.0 $g.L^{-1}$, species in order to provide growth conditions not limited by substrate availability.

CLSM datasets of the biofilms were acquired by staining with Syto 9 (Molecular Probes, Eugene, Oregon), a non-specific nucleic acid fluorescent probe. Vertical series (stacks) of images representing a horizontal cross section of 256 × 256 μm^2 at a resolution of 512 × 512 pixels were acquired at several time points during biofilm growth. Distance between adjacent optical sections in these stacks ranged from 1 μm to 2 μm, depending on the dataset. The number of cross sections in each of the stacks was that necessary to cover the full length of the biofilm thickness.

Two experimental datasets obtained from independent experimental runs performed using the same procedure but concerning different time ranges from inoculation were used for the comparative studies. Data from experiment 1 (**Exp1**) refers to four data points collected at times between 13 to 22 h after flowcell inoculation. Data from experiment 2 (**Exp2**), in turn, refers to five data points acquired between 24 and 40 h.

Using CLSM data as input to the model

CLSM datasets concerning **Exp1** at 13 h and **Exp2** at 24 h were used as input for simulations. For each voxel composing the 3D CLSM data a biomass particle was placed in the model initial state, with its mass being a function of the voxel greyvalue. To provide systematic conversion of greyvalues into biomass, the cumulative distribution of threshold values function (Xavier *et al.*, 2001), F, was used. F converts a greyvalue ($gv_{i,j,k}$) from the [0,255] range to the [0,1] range. As the greyvalues in CLSM datasets are dependent on hardware settings at the time of image acquisition, the use of F becomes imperative for accurate comparative studies. Greyvalues were converted to biomass using Eq. (3)

$$M_{x,y,z} = F(gv_{i,j,k}) \cdot \rho_{\text{biomass}} V_{\text{voxel}} \tag{3}$$

where $gv_{i,j,k}$ is the greyvalue of the voxel placed at entries (i,j,k) on the 3D matrix defined by the stack of images (discrete coordinates) and $M_{x,y,z}$ is the biomass at the corresponding position in continuous coordinates (x,y,z) (Table 1).

Simulations

The simulations were performed starting from initial model states defined as described above. Simulated biofilm structure was recorded at each time iteration of the model cycle,

Table 1 Model parameters

Variable	Value		Units	Description
	Exp 1	Exp 2		
$\rho_{biomass}$	70		$kg_{biomass}\ m^{-3}$	Biomass density
μ_{max}	6.94×10^{-5}	1.67×10^{-5}	s^{-1}	Biomass maximum specific growth rate (fitted)
D_S	1.6×10^{-9}		$m^2\ s^{-1}$	Substrate diffusivity
K_S	3.5×10^{-4}		$kg_{substrate}\ m^{-3}$	Saturation constant for substrate
K_{shov}	0.776	0.815	–	Shoving parameter (fitted)
V_{voxel}	2.5×10^{-19}	5×10^{-19}	m^3	Volume corresponding to one voxel
Y_{XS}	0.045		$kg_{biomass}\ kg_{substrate}^{-1}$	Biomass yield on substrate
C_S	State variable		$kg_{substrate}\ m^{-3}$	Substrate concentration
C_X	State variable		$kg_{biomass}\ m^{-3}$	Biomass concentration
$M_{particle}$	State variable		$kg_{biomass}$	Mass of one biomass particle

including mass and position of each biomass particle and the substrate concentration fields. Biofilm growth kinetics were fitted to the structure observed in data from **Exp1** and **Exp2** using minimization routines. The parameters μ_{max} and K_{shov} were fitted to the total biomass (B) and filled space fraction ($f(z)$) profiles (see below for definitions) of experimental data respectively, through a minimization procedure based on the Golden Section algorithm (Forsythe *et al*., 1977).

Quantitative comparison of 3D structures

The parameter set used for structure comparison is the following (Table 2):

- Filled space fraction, $f(z)$ also designated as "bacterial colonization" (Kuehn *et al*., 1998) or "solids hold-up" (Kreft *et al*., 2001) and linearly related to porosity (Xavier *et al*., 2003), is the fraction of area occupied by biomass at a given distance from the solid substratum.
- Total biomass per carrier area, B, is the sum of all biomass particles per analyzed area of solid substratum. For equivalence, B for experimental data is calculated using (4), derived from (3).

$$B = \sum_{i=1}^{128}\sum_{j=1}^{128}\sum_{k=1}^{128} F(gv_{i,j,k}) \cdot \rho_{biomass} V_{voxel} \tag{4}$$

- Substratum coverage, c_f, is the fraction of solid surface covered by the biofilm.
- Mean biofilm thickness, $\bar{Y}_f$, is the mean of height at which biofilm front rises above the solid surface.
- Biofilm surface roughness, σ, defined by (5)

$$\sigma = \sigma_f / \bar{Y}_f \tag{5}$$

Table 2 Biofilm structure parameters

Variable	Units	Description
$\bar{Y}_f$	m	Mean biofilm thickness
σ	–	Dimensionless biofilm surface roughness
B	$kg_{biomass}\ m^{-2}{}_{carrier}$	Total biofilm biomass per carrier area
c_f	$m^2{}_{biofilm}\ m^{-2}{}_{carrier}$	Biofilm colonization fraction at the solid substratum
$f(z)$	$m^2{}_{biofilm}\ m^{-2}{}_{carrier}$	Filled space fraction at distance z to the solid surface

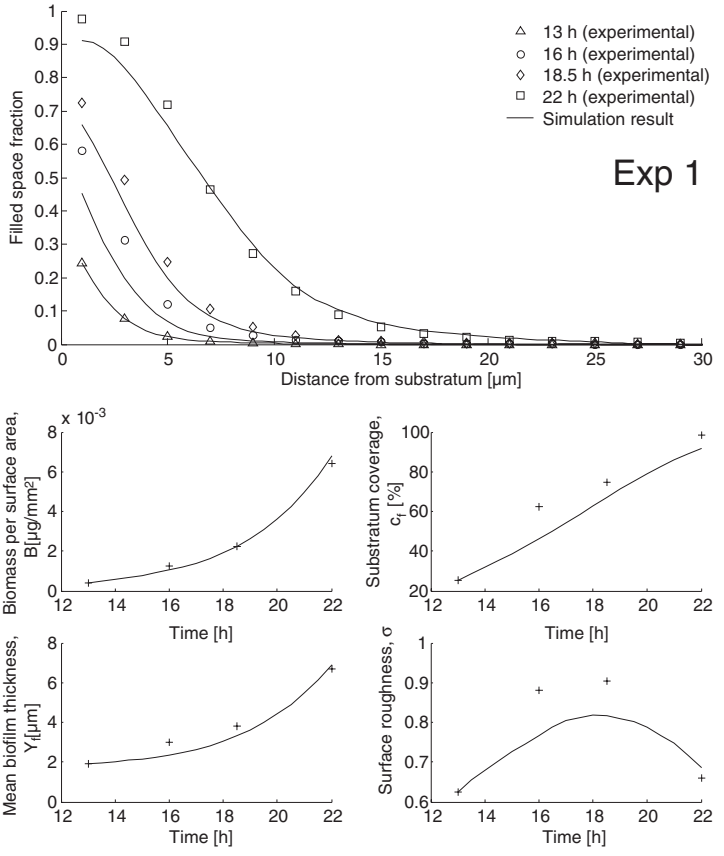

Figure 2 Comparison of experimental results from Exp1 with model predictions using $\mu_{max} = 0.25\ h^{-1}$ (best fit). Model fits filled space fraction profiles with $r^2 = 0.972$ and biomass per carrier area with $r^2 = 0.997$

where σ_f is the standard deviation of the height of biofilm front (Murga *et al.*, 1995; Picioreanu *et al.*, 1998).

All parameters (with the exception of B) concerning the structure predicted by the model were computed following re-discretization to a 128 × 128 × 128 grid of the spherical particles' position and radius.

Results and discussion

Biofilm growth regime

The initial experimental assumption that medium composition allowed for non diffusion-limited biofilm growth was confirmed by simulated substrate concentration fields. Minimum substrate concentration showed, in the worst case, decreases of about 10^{-4} % in relation to the bulk concentration, corresponding to irrelevant decreases in biomass growth rate.

Experimental observations

Data from **Exp1** show early biofilm development stages dominated by horizontal spreading throughout the carrier surface. Covering less than 25% of the surface at 13 h after inoculation, the biofilm spreads throughout the surface up to close to 100% at 22 h (Figure 2). For **Exp2**, at the initial monitored time (24 h) the biofilm occupies already more than 95% of the surface, and at 28 h the surface is completely covered by biofilm (Figure 3). For the case of **Exp2**, as the surface is fully covered for the duration of the monitored time range, growth along the vertical direction is much more significant than in **Exp1**.

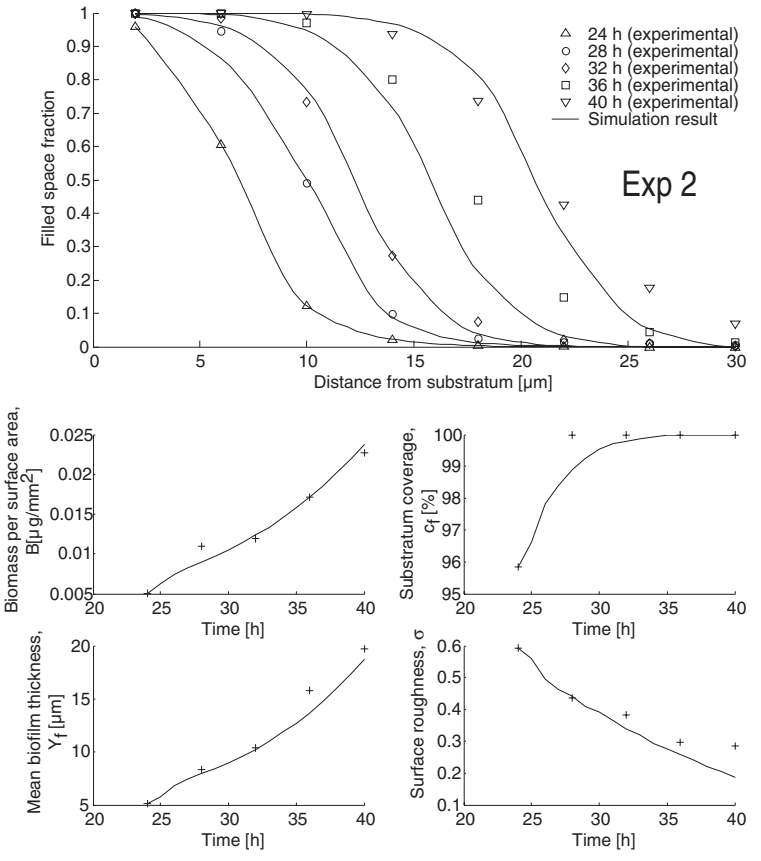

Figure 3 Comparison of experimental results from Exp2 with model predictions using $\mu_{max} = 0.06\ h^{-1}$ (best fit). Model fits filled space fraction profiles with $r^2 = 0.987$ and biomass per carrier area with $r^2 = 0.990$

Growth kinetics and morphology fit

Minimization of error of model prediction in relation to **Exp1** yielded $r^2 = 0.997$ in biomass correlation and $r^2 = 0.972$ in filled space fraction profiles. μ_{max} of 0.25 h^{-1} was estimated for the best fit (shown in Figure 2). Error minimization to results from **Exp2** yielded in turn $r^2 = 0.990$ in biomass correlation and $r^2 = 0.987$ in filled space fraction profiles. For this experiment, the estimated value for μ_{max} was 0.06 h^{-1} for the best fit (shown in Figure 3).

Modeling output fits well to the general trend of parameters measured from image analysis of CLSM data with the most significant differences being: (1) for **Exp1** underestimation of substratum coverage and of filled space fraction values closer to the solid surface and, for **Exp2**, slight underestimation of the mean biofilm thickness at 36 h.

Conclusions

1. CLSM imaging of biofilms provides an ideal source of data for the evaluation of 3-D biofilm models, due to its dynamic but non-destructive characteristics. For a quantitative comparison, the stochastic nature of biofilm development imposes the use of morphological parameters that can be readily evaluated by automated image analysis.
2. In spite of the different morphologies detectable in the two independent short-term experiments analyzed here, the model was capable of accurately fitting data from both experiments. Structure formation prediction was precise, as expressed by the set of morphology parameters used.
3. The observation that IbM biomass spreading rules accurately reproduce observed

biofilm structure addresses the previously stated concern that prediction of "normal" biofilm structure should first be established before full advantage can be taken of the potential of IbM (Kreft *et al*., 2001). This finding opens the way to the use of the IbM as a tool for biofilm modeling.

4. Preliminary results (data not shown) demonstrated that, although IbM and CA rules for biomass spreading produce equivalent structures, the former is computationally more demanding. In spite of this drawback, the IbM concept shows more promise, namely in the study of multispecies biofilm systems, and is one step closer to the aim of modeling biofilm formation from first principles.

Acknowledgements

Financial support by the F.C.T./M.C.T., Portugal, through the grant SFRH/BPD/11485/2002 is thankfully acknowledged.

References

Atkinson, B. and Davies, I.J. (1974). The overall rate of substrate uptake (reaction) by microbial films. Part I – A biological rate equation. *Trans. Instn Chem. Engrs*, **52**, 248–259.

Dockery, J. and Klapper, I. (2001). Finger formation in biofilm layers. *SIAM J. Appl. Math.*, **62**, 853–869.

Eberl, H.J., Parker, D.F. and van Loosdrecht, M.C.M. (2001). A new deterministic spatiotemporal continuum model for biofilm development. *J. Theor. Med.*, **3**, 161–175.

Forsythe, G.E., Malcom, M.A. and Moler, C.B. (1977). *Computer Methods for Mathematical Computations*. Prentice Hall, Englewood Cliffs.

Hermanowicz, S.W. (1999). Two-dimensional simulations of biofilm development: effect of external environmental conditions. *Wat. Sci. Tech.*, **39**(7), 107–114.

Hermanowicz, S.W. (2001). A simple 2D biofilm model yields a variety of morphological features. *Mathematical Biosciences*, **169**, 1–14.

Heydorn, A., Ersboll, B.K., Hentzer, M., Parsek, M.R., Givskov, M. and Molin, S. (2000). Experimental reproducibility in flow-chamber biofilms. *Microbiology*, **146**, 2409–2415.

Kreft, J.U., Booth, G. and Wimpenny, J.W.T. (1998). BacSim, a simulator for individual-based modelling of bacterial colony growth. *Microbiology*, **144**, 3275–3287.

Kreft, J.U., Picioreanu, C., Wimpenny, J.W.T. and van Loosdrecht, M.C.M. (2001). Individual-based modelling of biofilms. *Microbiology-Sgm*, **147**, 2897–2912.

Kuehn, M., Hausner, M., Bungartz, H., Wagner, M., Wilderer, P. and Wertz, S. (1998). Automated confocal laser scanning microscopy and semiautomated image processing for analysis of biofilms. *Appl. Environ. Microbiol.*, **64**, 4115–4127.

Lawrence, J.R., Wolfaardt, G.M. and Neu, T.R. (1998). The Study of Biofilms Using Confocal Laser Scanning Microscopy. Page 431 *in* M.H.F. Wilkinson and F. Schut (eds). *Digital Image Analysis of Microbes: Imaging, Morphometry, Fluorometry and Motility Techniques and Applications*. John Wiley & Sons, Chichester.

Murga, R., Stewart, P.S. and Daly, D. (1995). Quantitative analysis of biofilm thickness variability. *Biotech. Bioeng.*, **45**, 503–510.

Picioreanu, C., Loosdrecht, M.C.M. v. and Heijnen, J. (1998). Mathematical modelling of biofilm structure with a hybrid differential-discrete cellular automaton approach. *Biotech. Bioeng.*, **58**, 101–116.

Picioreanu, C., van Loosdrecht, M.C.M. and Heijnen, J.J. (1999). Discrete-differential modelling of biofilm structure. *Wat. Sci. Tech.*, **39**(7), 115–122.

Picioreanu, C., van Loosdrecht, M.C.M. and Heijnen, J.J. (2000). Effect of diffusive and convective substrate transport on biofilm structure formation: A two-dimensional modeling study. *Biotechnology and Bioengineering*, **69**, 504–515.

Pizarro, G., Griggeath, D. and Noguera, D.R. (2001). Quantitative cellular automaton model for biofilms. *Journal of Environmental Engineering*, **127**, 782–789.

Press, W.H., Flannery, B.P., Teukolsky, S.A. and Vetterling, W.T. (1993). *Numerical Recipes in C: the Art of Scientific Computing*, 2nd edition. Cambridge University Press, Cambridge.

Rittman, B.E. and McCarthy, P.L. (1980). Model of steady-state biofilm kinetics. *Biotechnol. Bioeng.*, **59**, 261–272.

van Loosdrecht, M.C.M., Heijnen, J.J., Eberl, H.J., Kreft, J.U. and Picioreanu, C. (2002). Mathematical modelling of biofilm structures. *Antonie van Leeuwenhoek*, **81**, 245–256.

Wanner, O. and Gujer, W. (1986). A multispecies biofilm model. *Biotech. Bioeng.*, **28**, 314–328.

Wanner, O. and Reichert, P. (1996). Mixed modeling of mixed-culture biofilms. *Biotechnol. Bioeng.*, **49**, 172–184.

Wimpenny, J.W.T. and Colasanti, R. (1997). A unifying hypothesis for the structure of microbial biofilms based on cellular automaton models. *FEMS Microbiol. Ecol.*, **22**, 1–16.

Xavier, J.B., Schnell, A., Wuertz, S., Palmer, R., White, D.C. and Almeida, J.S. (2001). Objective threshold selection procedure (OTS) for segmentation of scanning confocal laser microscopy images. *J. Microbiol. Meth.*, **47**, 169–180.

Xavier, J.B., White, D.C. and Almeida, J.S. (2003). Automated Biofilm Morphology Quantification from Confocal Laser Scanning Microscopy Imaging. *Wat. Sci. Tech.*, **47**(5), 31–37.